AIMS Materials Science, 4(1): 43-60.
DOI: 10.3934/matersci.2017.1.43
Received: 31 October 2016
Accepted: 15 December 2016
Published: 21 December 2016

http://www.aimspress.com/journal/Materials

Research article

The hybrid nanobiointerface between nitrogen-doped graphene oxide and lipid membranes: a theoretical and experimental study

P. Di Pietro [1], G. Forte [2,*], L. D'Urso [3], and C. Satriano [1,*]

[1] Nanobiohybrid Interfaces Laboratory (NIL), Department of Chemical Sciences, University of Catania, Viale Andrea Doria, 6, I-95125 Catania, Italy
[2] Department of Pharmaceutical Sciences, University of Catania, Viale Andrea Doria, 6, I-95125 Catania, Italy
[3] Department of Chemical Sciences, University of Catania, Viale Andrea Doria, 6, I-95125 Catania, Italy

* **Correspondence:** Email: gforte@unict.it; csatriano@unict.it.

Abstract: In this study, we present a comparison between graphene oxide (GO) and nitrogen-doped GO (N-GO) in terms of spectroscopic properties and biomolecule-binding potentiality features. Specifically, GO nanosheets, both in aqueous dispersion and in solid state, were successfully modified with different amino-containing moieties, in order to obtain graphene-based nanostructures able to respond to chemical stimuli (e.g., pH) and with tunable surface properties. The physisorption of dye-labelled lipid vesicles loaded with curcumin, was scrutinised both theoretically and experimentally. The energetics of the hybrid lipid membrane-curcumin-GO interface at different pH values, representative respectively of physiological (7.4) and pathological (5.5) environment, were estimated by molecular dynamics (MD) simulations. The GO and GO-N samples characterization by Raman, fluorescence, and UV-vis spectroscopies, as well as confocal microscopy demonstrated promising features of the (N-)GO/lipid platforms for fluorescence imaging and drug delivery applications.

Keywords: 2D nanomaterials; supported lipid bilayers; surface functionalisation; molecular dynamics; confocal microscopy

1. Introduction

The nano-biointerfaces established between graphene oxide (GO) and biomolecules attracted in the last years an increasing interest, for both fundamental [1] and application research, including biosensing [2], drug-delivery [3], theranostics [4], cancer therapy [5], biotechnology and biodevices [6]. The large surface area and the combination of hydrophobic character and π-π stacking interaction with drug molecules are some reasons for the interest of graphene application in theranostics [7,8]. On the other hand, graphene oxide, exhibits a unique set of properties, arising from oxygen functional groups, thus enabling its solubility in a variety of aqueous solvents and offering a route towards derivatization with other chemical moieties. The functionalization of graphene by using organic moieties constitutes an affordable way to modulate its physical and chemical properties, especially at the interface with biomolecules. Indeed, GO, covalently decorated (either on the basal plane or at the edges) with oxygen-containing functional groups (carboxyl, hydroxyl, epoxide and carbonyl) provides many opportunities through the manipulation of the size, shape and relative fraction of the sp^2-hybridized domains of GO by reduction chemistry [9].

The surface termination of GO is especially relevant for the applications of graphene-based materials in the biomedical area, where several pre-requisites and the possibility of different toxicological effects need to be considered. In particular, toxicity depends on the surface features (the chemical structure or the nature of functionalized coating), size, number of layers, cell type, administration route (for *in vivo* experiments), dose time of exposure and synthesis methods. To this end, development of suitable chemical synthesis and functionalization approaches to precisely control the characteristics of graphene is urgently needed [7]. With the rapid growth in the application of GO at the biointerfaces, the toxicity of GO toward bacterial and mammalian cells has recently attracted extensive research attention [10]. The propensity for GO to attach to and disrupt model cell membranes using supported lipid bilayers (SLBs) and supported vesicular layers (SVLs) has been used to scrutinize possible mechanisms for the cytotoxicity of GO [11] and, in general, as model of a solid-liquid nanobiointerface to study the interaction of engineered nanomaterials with the biological membranes [12,13].

Among the various approaches used for the doping of graphene, the introduction of amino groups is one of the most attractive to control the charge-potential landscape at solid-liquid interfaces, for engineered novel devices for applications in catalysis and energy conversion as well as sensing and biodevices. For example, amino-functionalized reduced graphene oxide was demonstrated as feasible and effective strategy to solve the long-term cycling difficulty for lithium-sulphur batteries [14]. Moreover, GO sheets functionalized by aminopropylsilyl groups and labelled by Au nanoparticle radioisotopes were used for fast *in vivo* targeting and imaging of tumours [15].

Methods used for the synthesis of nitrogen-functionalized graphene nanosheets include the grafting of alkylamines [16], the selective alkylation/basic hydrolysis reactions using the nitrogen precursor bromoacetonitrile [17], the Bucherer-type reaction under hydrothermal conditions [18].

A theoretical study about the thermal stability and thermodynamics of amino- and ethylamino-graphene found that more amino groups stabilize the functionalized graphene thus favouring further amination, whereas a small concentration of amino groups is unstable in many cases [19]. The isoelectric pH of graphene, less than 3.3, can be changed up to 7.5 by non-covalent electrochemical attachment of aromatic amino groups, preserving the favourable electronic properties of graphene throughout [20].

The interaction between GO and lipid membranes, using both supported lipid membranes and supported liposomes undisclosed that graphene oxide induces the rupture of pre-adsorbed liposomes and the formation of a nanocomposite, bio-nonbio multilayer structure, consisting of alternating graphene oxide monolayers and lipid membranes, with an important role played by electrostatic interactions between graphene oxide and lipid headgroups [13]. For instance, Wu et al., provided evidence that overcoming the electrostatic repulsion of phosphate group, its hydrogen bonding attraction as well as the electrostatic and hydrophobic interaction of choline group are the driving forces for the effective adsorption of GO on lipid membrane [21]. However, so far, a comprehensive understanding about the nature of the interaction between GO and lipid membrane still remains challenging.

In the present study, we address a comparative investigation of GO and nitrogen-doped GO (N-GO) at the hybrid nano-biointerface with lipid bilayers at the two pH of 7.4 and ~6. To the best of our knowledge, this paper provides the first investigation, both theoretical and experimental, of the interaction between N-GO and lipid membranes.

The effect of the graphene-lipid biointerface for drug delivery applications was scrutinized by using the case study of curcumin (Curc), a natural yellow pigment isolated from the turmeric plant. Curc has a variety of biological activities and pharmacological actions, such as anti-inflammatory, anti-carcinogenic, and anti-virus properties, as well as promising clinical applications due to the low toxicity [22]. However, the extremely low aqueous-solubility of curcumin and the rapid intestinal and hepatic metabolism result in poor systemic bioavailability of the drug. Lipid vesicles provide a convenient nanocarrier platform to vehicle and deliver the drug [23]. Here, we demonstrate that a controlled modification of the GO surfaces by introducing amino-containing groups at different oxidation level, can modulate the surface termination and, in turn, the release of curcumin at the graphene surfaces from lipid vesicles loaded with the model drug.

2. Materials and Methods

2.1. GO Fabrication

Graphene sheets were deposited on glass or silica by mechanical exfoliation of graphite and successively exposed to UV-ozone (UVO) irradiation for 1 h [24]. Alternatively, GO was synthesized from graphite powder using a modified Hummer's method [25]. In brief, 0.5 g of graphite and 0.5 g of sodium nitrate were mixed together followed by the addition of 23 mL of conc. sulphuric acid under constant stirring. After 2–3 minutes under stirring, 3 g of $KMnO_4$ was added slowly to the above solution while keeping the temperature less than 20 °C to prevent overheating and explosion. The mixture was stirred at 35 °C for 1 h and the resulting solution was diluted by adding 40 mL of water under vigorous stirring. To ensure the completion of reaction with $KMnO_4$, the temperature was increased until 90 °C for 30 minutes. The suspension was further treated with 30% H_2O_2 solution (5 mL). The resulting mixture was washed with HCl and H_2O respectively, followed by filtration and drying. Graphene oxide sheets were thus obtained.

2.2. Preparation of N-GO

GO dispersion: 500 μL of GO dispersion (0.4 mg/mL) was treated for 2 h under vigorous stirring (1300 rpm at 25 °C) with 1 mL of dodecylamine (DDA, 4.8 mM in ethanol), or 50 μL of hydrazine (N_2H_4, 32 M) to prepare the GO-DDA and GO-N_2H_4, samples, respectively. The GO-DDA/N_2H_4 sample was prepared by the addition of 50 μL of N_2H_4 to GO-DDA and the dispersion was kept under stirring overnight [26]. *GO solid*: 1 mL of GO (0.4 mg/mL) was deposited and dried at the air on glass bottom Petri dishes (WillCo Wells). Then, 500 μL of DDA (3.2 mM), or N_2H_4 (1 M), or DDA/N_2H_4 mixture were added. After drying by solvent evaporation, samples were washed with ultrapure water (X2) and dried under argon flux.

2.3. Preparation of the Lipid Vesicles

Zwitterionic small unilamellar vesicles (SUVs) were prepared from a 5 mg/mL chloroform solution of 1-palmitoyl-2-oleoyl-sn-glycero-3-phosphocholine (POPC, Avanti Polar Lipids Inc., US) added (1 wt%) with rhodamine-DHPE (1,2-dihexadecanoyl-sn-glycero-3-phosphoethanolamine, Avanti Polar Lipids Inc., US) to obtain dye-labelled POPC-Rhod. To prepare the curcumin loaded vesicles (POPC-Rhod-Curc), 1 mg of curcumin was dissolved into the lipid solution in chloroform. The solvent was evaporated under Ar flow, to obtain lipid films adsorbed on the wall of a round-bottomed flask. The film afterward was emulsified in 1 mL of phosphate buffer saline solution (PBS, 0.01 M phosphate buffer containing 0.003 M KCl and 0.14 M NaCl, pH 7.4 at 25 °C) at room temperature, vortexed, and extruded 13 times through a 100 nm polycarbonate membrane, followed by another 13 times through a 30 nm membrane (Avanti Polar Lipids Inc., AL, US). In order to remove the unloaded curcumin, the vesicles were centrifuged 15 min at 8,000 rpm and the supernatant recovered and stored under Ar at 4 °C.

2.4. UV-Visible (UV-Vis) and Fluorescence Spectroscopy

UV-Vis spectra for all samples were recorded in quartz cuvettes with 1 cm optical path length on a Jasco spectrometer. Fluorescence spectra were acquired on a Perkin Elmer LS55 by using a quartz cuvette with an optical path length of 1 cm. Emission and excitation spectra were acquired fixing the wavelength respectively at the 405 nm and 620 nm emission, with excitation slits ($slit_{ex}$) and emission slits ($slit_{em}$) aperture of 6 nm and 4 nm, respectively.

2.5. X-ray Photoelectron Spectroscopy (XPS)

XPS measurements were performed using a PHI 5000 VersaProbe apparatus equipped with a monochromatic Al source (1486.7 eV). Typically, the pressure in the analysis chamber was 5×10^{-9} Torr. Dual beam charge neutralization from an electron gun (~1 eV) and the argon ion gun (<10 eV) were used for charge compensation on the sample surface during the measurements. X-ray (10 kV, 22 mA) beam was produced using an aluminum anode and had a spot size of 250 × 1000 μm. Wide-scan and narrow scans spectra were recorded at a resolution of 0.5 eV and 0.1 eV, respectively. A Shirley background was subtracted by all spectra, and peak fitting was performed using a Gaussian

function. The binding energy were calibrated assuming the major component of the C1s peak to result from hydrocarbon contribution at the binding energy of 284.6 eV.

2.6. Raman Spectroscopy

Raman spectra were excited using the 514.5 nm radiation of an Ar ion laser and analysed using a Jobin Yvon 450 nm focal length monochromator, equipped with a CCD camera detector cooler at 77 K.

2.7. Confocal Microscopy and Fluorescence Recovery after Photobleaching (FRAP) Measurements

An Olympus laser scanning confocal microscope (FV1000 model) was used, equipped with diode UV (405 nm), multiline Argon (457 nm, 488 nm, 515 nm) HeNe (G/R) (543/633 nm) lasers. An oil immersion objective (60×O PLAPO) and spectral filtering system were used. The detector gain was fixed at a constant value and images were taken, in sequential mode, for all the samples at random locations throughout the area of the well.

For FRAP analyses, snapshots were acquired as follows: three images before bleach, then bleaching by using a high intensity (95% power) Ar laser, and other micrographs every 5 seconds up to 2 minutes. By translating the sample stage, an average of 10 spots per substrate was photobleached in a given experiment. FRAP curves were analysed by Image J software (NIH, US). The data were normalized to the initial (pre-photobleach) value, which enabled the percentage of photobleaching and the percentage fluorescence recovery within the laser region to be determined. For each sample, the emission recorded from the bleached spots was compared with that coming from contiguous non-bleached areas.

2.8. Computational Methods

The Klinowsky model was followed to build graphene oxide (GO) [27]. Following such scheme hydroxyl and epoxy groups are mainly present and randomly distributed on both sides of the sheet. A partial oxidized GO was taken into account, meaning that 1 epoxy group and 1 hydroxyl group per 10 C atoms are considered. GO-NH_2 was obtained by substitution of all hydroxyl groups on the surface with amine groups. Similarly GO-dodecylamine was built starting form GO and replacing –OH with $–NH(CH_2)_{11}CH_3$.

One molecule of curcumin was inserted into a double layer of POPC. Since DFT calculations have shown that the enolic form of curcumin is lower in energy than the diketone of 36.76 kJ/mol, the former was considered in all simulations.

Ab initio calculations were performed in the framework of the DFT using the Perdew–Burke–Ernzerhof functional [28] with the 6-311+(d, p) basis set [29,30].

A water layer, whose thickness was about 1.2 nm, was placed between the considered surfaces and the Curc-POPC system. A further layer of water with the same thickness was finally placed onto the double layer.

In order to simulate the pH effect –OH groups in GO were considered deprotonated at pH = 7. On the other hand, we have assumed that $–NH_2$ and –NHR groups were protoned at pH = 5.

For MD simulations we have followed a scheme previously adopted [31], in detail all the simulation were performed under Periodic Boundary Condition in a box of 25 × 125 × 25 nm adopting the Consistence Valence Force Field parameterization together with CVFF flexible water potential [32,33]. To integrate the equation of motion a time step of 1 fs was chosen and simulations were run under NVT conditions at 298 K (Berendsen thermostat was used with a decay constant of 1 ps). Long range electrostatic interactions were calculated through the particle-mesh-Ewald method.

The structures were first of all optimized applying 10000 steps of conjugate gradient algorithm to the water molecules, fixing the solute; this was followed by 20-ns of MD of the solvent and finally 40-ns of MD were performed removing the constraint and during this time the data were collected for analysis. In all cases the charge neutrality is maintained by using Na^+ and Cl^- as counterions. In POPC the negative charge of phosphate was always counterbalanced by positive ammonium salt, hence the double layer is neutral.

3. Results and Discussion

3.1. Preparation of N-GO Derivatives and Spectroscopic Characterization

The amino-derivatisation of GO samples was studied by using two different approaches of wet chemistry reduction. In the first approach N-GO in dispersion was produced by adding the reductant agents (N_2H_4, DDA or DDA/N_2H_4 mixtures) to the aqueous dispersion of the graphene oxide. In the second approach, N-GO solid was obtained by deposition, through exfoliation of graphite, of numerous sheets of graphene on a silica substrate, then oxidising graphene to graphene oxide by UVO treatment and eventually dropping the reducing solutions at the top surface of the GO solid samples. The Raman spectra of the solid state samples used in the second approach are shown in Figures 1 and S1 in ESI.

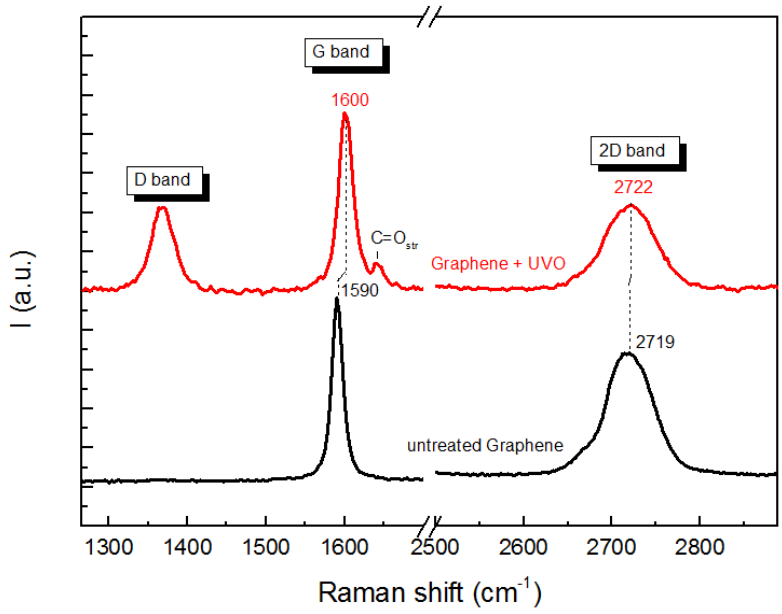

Figure 1. Raman spectra of a few layer-thick graphene sample before (black line) and after (red line) oxidation by UVO (treatment time = 1 h).

The spectra of a few-layers thick (~5 layers) graphene (FLG) sample, before and after exposure to UVO, demonstrates the effectiveness of 1 h treatment for the conversion of the original graphitic structure to an oxidised form (Figure 1). Indeed, the spectrum of untreated graphene shows a unique peak, at about 1590 cm^{-1}, characteristic of sp^2 carbon (G band), whereas for the UVO-treated graphene two new peaks are visible, at ~1350 cm^{-1}, typical of sp^3 carbon (D band), and at ~1620 cm^{-1}, due to carbonyl stretches [34]. The shape and the position of the 2D band that usually can be used to determine the stacking order in a FLG, can also be related to the possible stress and defects induced by the UVO treatment. There is no significant change in spectral shape of the 2D band but only a negligible decrease in the peak intensity.

To investigate the in-depth effect of the UVO-induced oxidation of the graphene sheets, samples at different thicknesses, corresponding to a low (~2), a medium (~5) and a high (~10) number of graphene layers, i.e., the layer numbers of the graphene sheets, were deposited on silicon, exposed to UVO for 1 h and therefore analysed by Raman spectroscopy. Figure S1 shows the comparison of graphene samples deposited at different thicknesses (Figure S1a) and those of graphene samples converted to GO by UVO treatment (Figure S1b).

The reduction of GO by dodecylamine is expected to introduce amino functionalities at the near interface with the graphene sheet, thus resulting in N-GO samples with an outward orientation of alkyl groups, e.g., C(graphene sheet) = NH–$(CH_2)_{11}CH_3$. In the case of hydrazine, the bifunctional character of the molecule is likely to prompt the formation of N-GO aggregates, with diazo moieties (e.g., C(graphene sheet 1) = N–N = C(graphene sheet 2) bridging between two or more graphene sheets. When both DDA and N_2H_4 are used, the dodecylamine molecules may play a spacer role between the graphene sheets, and therefore the presence of amino-terminated graphene sheets can be figured out, e.g., C(graphene sheet) = N–NH_2 (Figure 2).

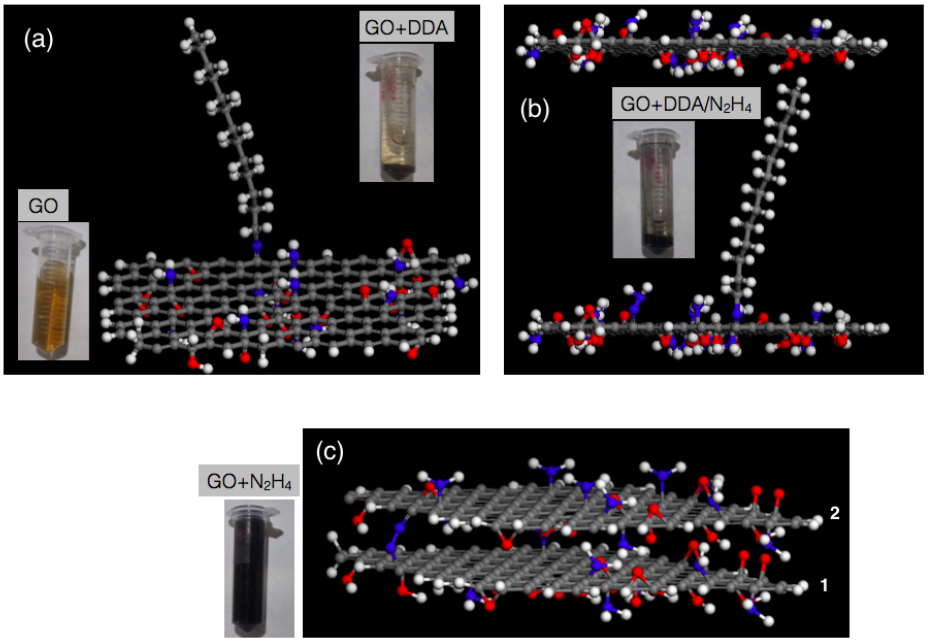

Figure 2. A schematic view (and photographs of the prepared samples) for the three different N-doped GO obtained by GO treatment with: (a) DDA, (b) N_2H_4, (c) DDA/N_2H_4.

The Raman spectra of N-GO samples obtained in the two used approaches, dispersion or solid state, are reported in Figure S2 in ESI.

The optical characterisation of GO and of N-GO samples in dispersion prepared by reduction with DDA, N_2H_4 and DDA/N_2H_4 confirm that different interactions occurr at the interface between the functionalised GO samples and aqueous solutions. It must be noted that while hydrazine is a known reductant of GO, the interaction between GO and DDA has three possibilities: hydrogen bonding, electrostatic attraction between carboxylic group and protonated amine and, most predominantly, the nucleophilic substitution between epoxy and amine, which result into the grafting of the long hydrocarbon chain of the octadecylamine onto GO sheets [26,35].

Indeed, Figure 3 shows, for all the N-GO samples, a bathochromic shift of the GO characteristic spectral features, which are the peak around 230 nm (π-π* plasmon peak [36]) and the shoulder around 300 nm [37]. Similar trends are found both in water (pH: ~6, Figure 3a) and in PBS buffer (pH: ~7.4, Figure 3b). In particular, the peak at 230 nm exhibits a red shift of about 29 nm in GO + N_2H_4 sample, both in water and in buffer. In GO + DDA sample such a peak disappears in water and broadens in PBS. As to the sample GO + DDA/N_2H_4, a sum effect of contributions of the GO + DDA and GO + N_2H_4 spectra is observed.

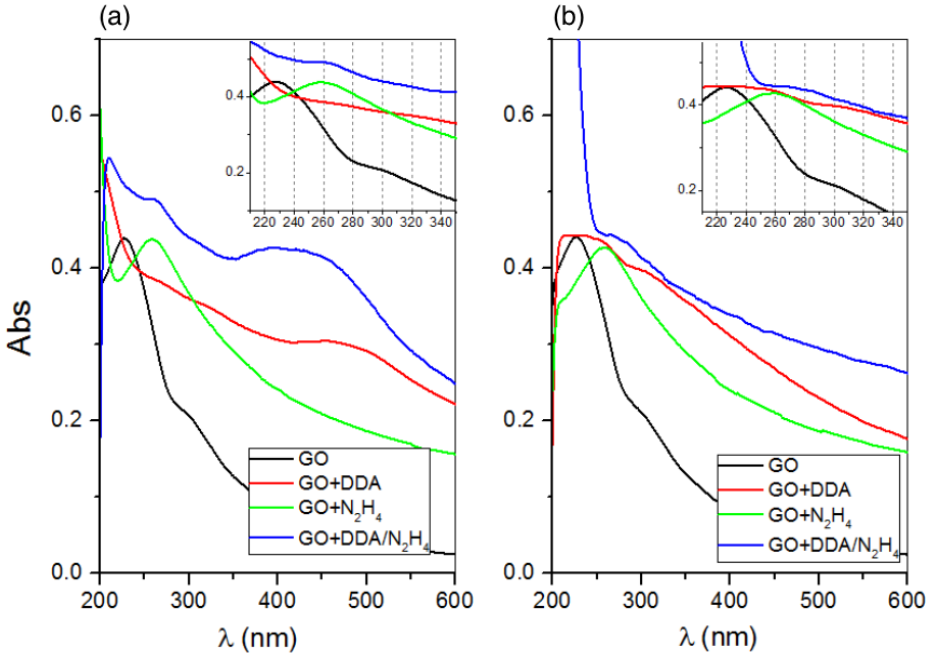

Figure 3. UV-Vis spectra in ultrapure water (a) or PBS buffer (b) of GO and N-GO samples obtained by treatment with dodecylamine (GO + DDA), hydrazine (GO + N_2H_4) or the mixture (GO + DDA/N_2H_4).

In the the π-π* plasmon peak two kinds of conjugative effect coexist, related to nanometer-scale sp^2 clusters and linking chromophore units such as C=C, C=O and C–O bonds [37]. The UV-Vis spectral changes in N-GO samples in comparison to GO can be related to the introduciton of defects in the sp^2 domains by the formation of new C=N bonds, as well as conjugative effect of chromophore aggregation, which influences the π-π* plasmon peak.

The average surface atomic composition (Table 1) obtained by XPS analyses and the deconvolution of C1s and N1s peaks (Figure 4) confirm the considerations inferred from the UV-Vis spectra. Indeed, the relative intensity ratio C1/C2/C3 of the different components of carbon peak in GO, respectively at 284.6 eV (C1, C–C and C–H bonds), 286.7 ± 0.2 eV (C2, C–O bonds) and 288.7 ± 0.2 eV (C3, C(=O)O bonds) of binding energy (BE), change differently in the different GO-N samples, which all exhibit a new C=N component (C4, at 285.7 ± 0.2 eV [38]). Compared to the spectrum of GO, the decrease of peak intensity of C2 component in GO + DDA (Figure 4b) and GO + N_2H_4 (Figure 4c) indicates that the grafting mainly occurred through the reaction of the epoxide functional group in GO. In the case of GO + DDA, a component related to the carbonyl groups is found (C5, at 288.2 ± 0.2 eV) instead of the carboxylic C3 component.

Table 1. Quantitative analysis in atomic percentage from XPS analysis of bare and amino-GO derivatives.

	C1s (at%)	O1s (at%)	N1s (at%)	N/O
GO	71.8	28.2	-	0
GO + DDA	80.2	16.7	3.1	0.2
GO + N_2H_4	80.3	13.4	6.3	0.5
GO + DDA/N_2H_4	71.1	25.6	3.2	0.1

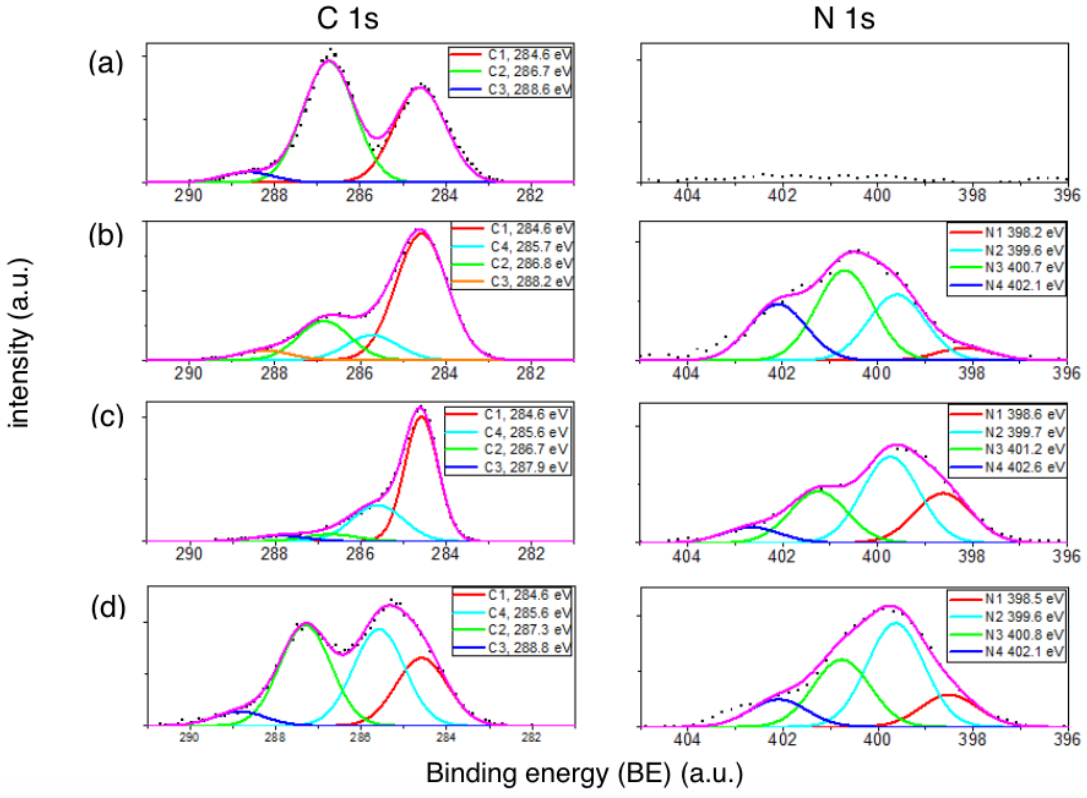

Figure 4. XPS spectra of C1s (left panels) and N1s (right panels) regions for: (a) GO; (b) GO + DDA, (c) GO + N_2H_4, (d) GO + DDA/N_2H_4.

As to the nitrogen XPS spectra of the different nitrogen-doped GO surfaces, the broad N1s peak could be deconvoluted into four chemically shifted components: at 398.8 ± 0.2 eV (N1), 399.6 ± 0.2 eV (N2), 400.7 ± 0.2 eV (N3) and 402.1 ± 0.2 eV (N4) of binding energy, respectively. These peaks are assigned respectively to: hydrogen-based interactions between the amino groups and the oxygen functionalities (N1), C–N linkages as a result of covalent interactions of amino groups with GO (N2), charge-induced interactions between the protonated amines and weakly acidic sites of GO (N3), and $C–N^+$ (from quaternary nitrogen) or NH_4^+ (N4) [39]. The N2 component is therefore an indicator of the effective grafting of the *n*-alkylamines on the basal plane of GO through covalent interactions, whereas the structurally strained epoxy groups are unzipped by the nucleophilic substitution of *n*-alkylamines [40]. Some of the amines interact with the oxygen functionalities *via* hydrogen bonding as supported by the appearance of the N1 component. The weak acidic sites such as the carboxyl and phenolic groups interact with the amino groups through columbic interactions, induced by the transfer of H^+, as revealed by the N3 component.

3.2. The Interaction of GO and N-GO Derivatives with Curc-loaded Lipid Membranes: Theoretical Calculations

Curcumin–GO–NH_3^+ (simulation at pH = 5) and GO–NH_2 (simulation at pH = 7). The mobility of curcumin inside the bilayer is represented in Figure 5, where the distance between N-GO surface and the phenolic oxygen of curcumin ($d_{N\text{-}GO/OH(Curc)}$) is reported.

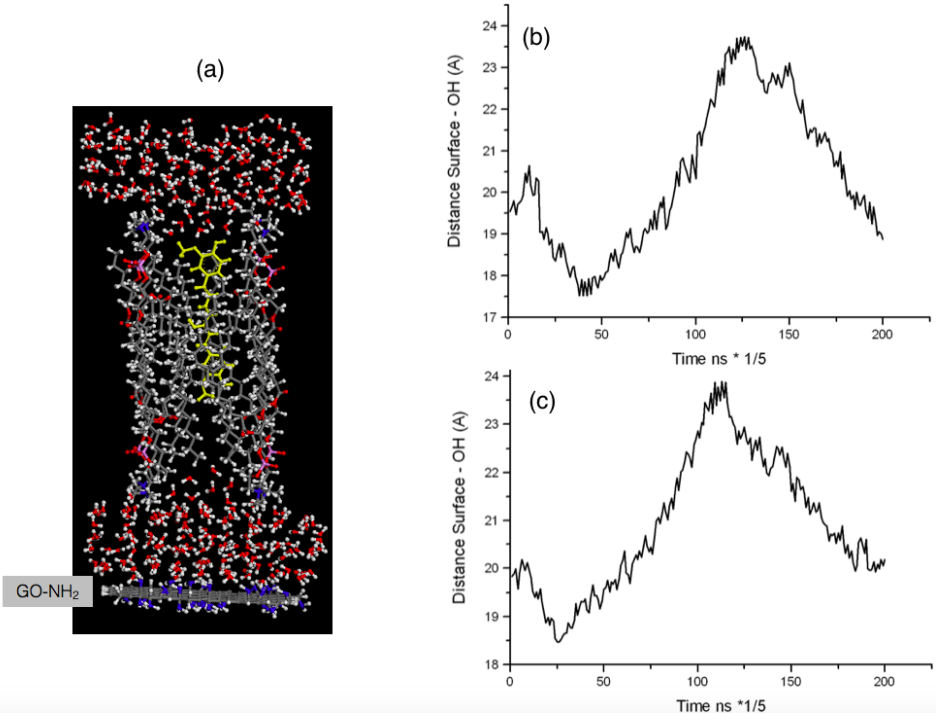

Figure 5. Curcumin intercalated in the POPC bilayer (a; carbon atoms are shown in grey, nitrogen atoms in blue and oxygen atoms in red spheres, curcumin molecule atoms are in yellow) and calculated distance between the amino-terminated N-GO surface and the phenolic oxygen of curcumin floating within the top and bottom leaflets of the lipid bilayer: (b) pH = 7; (c) pH = 5.

In the model used for this study, curcumin in the linear enolic form, more stable than the bent dichetonic form, intercalated into the supported lipid bilayer. Water molecules rest at the two leaflets surfaces, both at the top and at the interface with the graphene substrate (Figure 5a). To model the N-GO substrate with the amino groups at the outward surface, each hydroxyl group is replaced with amino groups; depending on the pH, the modelled N-GO surface exposes neutral amino (at pH = 7), or positively charged quaternary ammonium (at pH = 5).

It is interesting to note that for both the pH, the distance $d_{N\text{-}GO/OH(Curc)}$ is subjected to wide fluctuations, which basically span the 5 nm of the bilayer thickness, even if the molecule remains included in the double layer. However, at the pH of 7 (Figure 5b), the amplitude of oscillation is a bit higher, thus the curcumin emerges from the bilayer presenting the hydroxyl towards the water. Moreover, we can observe smooth minimum and maximum values (respectively at around 40 and 125 ns in Figure 5a) where the distance from the surface remains constant for a while, owing to the strong electrostatic interaction that involves the negatively charged phosphate groups and H bonds with the water and the carbonylic group of the POPC. At this value of pH, a random orientation of the water molecules is found (Figure 6). Significant differences are observed in the simulations at pH = 5 (Figure 5c), where the fluctuations and the absolute distance between Curc and N-GO surface are smaller in comparison to pH = 7. However, maximum and minimum values are quite sharp, suggesting a reduced mobility of curcumin into the double layer and phenolic hydroxyl be kept away from the layer of water.

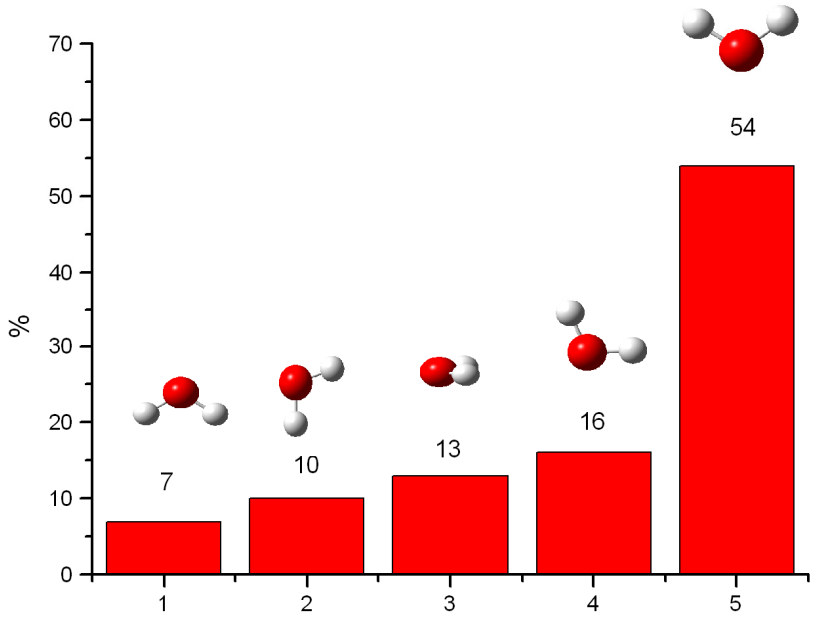

Figure 6. Orientation of water at the GO interface.

It must be noted that the orientations of water molecules seem to be influenced by positive charges ($GO–NH_3^+$) located on the surface. Since long range electrostatic interactions, the negative side of the dipole associated to the water molecules mostly point toward the surface giving rise to a "V" prevailing orientation (Figure 6). As a consequence, the positive charge of the dipole,

characterized by the hydrogen atoms, repels the partially positive charged hydrogen atom of the phenolic group (Ph–OH) pushing away the curcumin inside the double layer.

Being due to the GO–NH_3^+ surface, such arrangement is not present in the water layer placed above the double layer. In fact, a random orientation of the dipoles is found in this layer therefore any repulsive effect, with respect to the Ph–OH group is observed.

The mobility of curcumin within the POPC bilayer at the interface with N-GO samples obtained by GO + DDA treatment as well as with GO is represented in Figure 7.

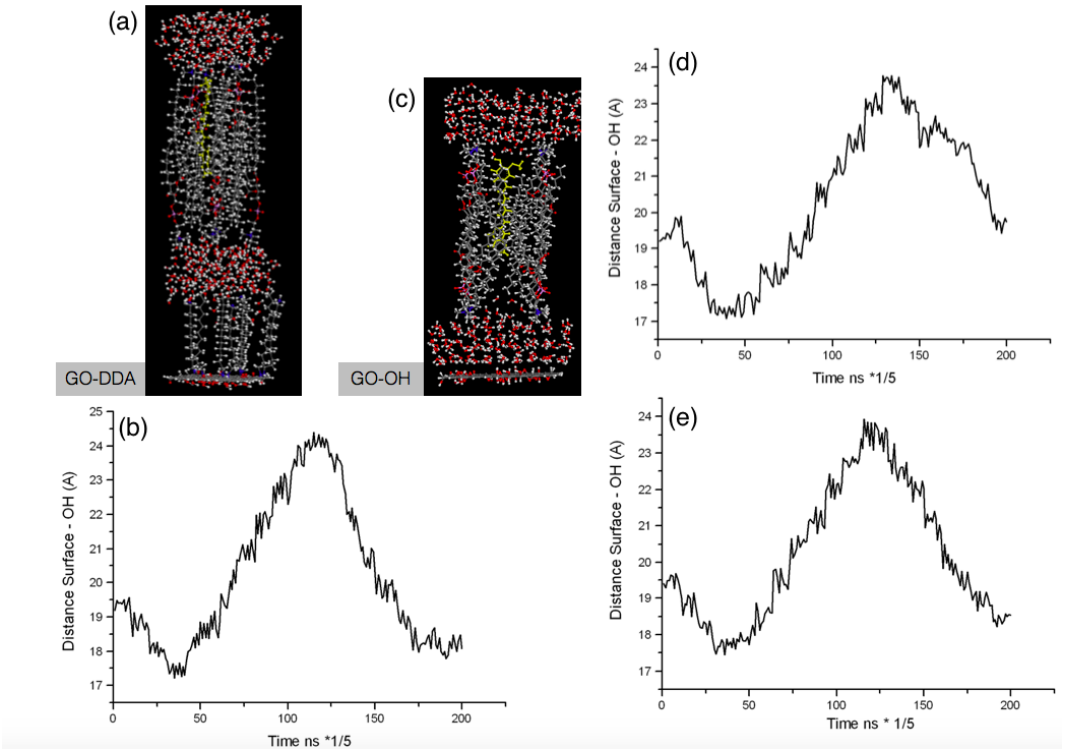

Figure 7. Calculated distance between the phenolic oxygen of curcumin floating within the top and bottom leaflets of the lipid bilayer and: (a, b) methyl-terminated N-GO surface; (c) hydroxyl-terminated GO surface at pH = 7 (d) and pH = 5 (e).

Curcumin–GO–$NH(CH_2)_{11}CH_3$ (Figure 7a). The simulations at pH = 5 and pH = 7, show a negligible effect of pH and a very low affinity between the functionalized surface and water layer, which give rise to desorption of the entire system from the surface (Figure 7b). In fact, the layer of water and the nitrogen atoms in dodecylamine, which are directly bound to GO, are separated by a large distance.

Curcumin–GO–OH (Figure 7c). As pointed out above, at neutral pH the –OH groups in GO were considered deprotonated (GO–O^-). The overall effect is that the dipole associated to water molecules is oriented in a opposite way if compared to GO–NH_3^+. In the layer between surface and POPC water molecules are mainly oriented with the positive side of the dipole toward GO–O^-. It follows that phenolic hydrogen atom of curcumin undergo an attractive interaction and, at the end of the side, its distance from the surface remains constant for a while (Figure 7d). Any relevant effect is observed in the proximity of the layer above POPC. At acid pH, the picture is essentially similar to

GO–NH_2. Also in this case, a random orientation of dipole moment is detected and the mobility of curcumin is characterized by wide fluctuations (Figure 7e).

3.3. The Interaction of GO and N-GO Derivatives with Curc-loaded Lipid Membranes: Experimental Results

An experimental validation of theoretical calculations discussed in the previous section on the mobility of the curcumin within the POPC lipid bilayer at the interface with the different GO substrates was performed by confocal microscopy and FRAP analyses to assess whether the drug incorporation into the membrane could affect its fluidity. In fact, the lateral mobility of the lipid molecules within the membrane, quantified by the diffusion coefficient D at the solid interface, is an important indicator of the drug loading and release capabilities by the lipid bilayer platform. Supported lipid bilayers of rhodamine labelled POPC (PC-Rhod) and curcumin-loaded POPC (PC-Rhod-Curc) lipids were obtained by physical adsorption of the lipid vesicles on a hydrophilic glass followed by spontaneous rupture/fusion of the vesicles and the formation of the supported membranes [41].

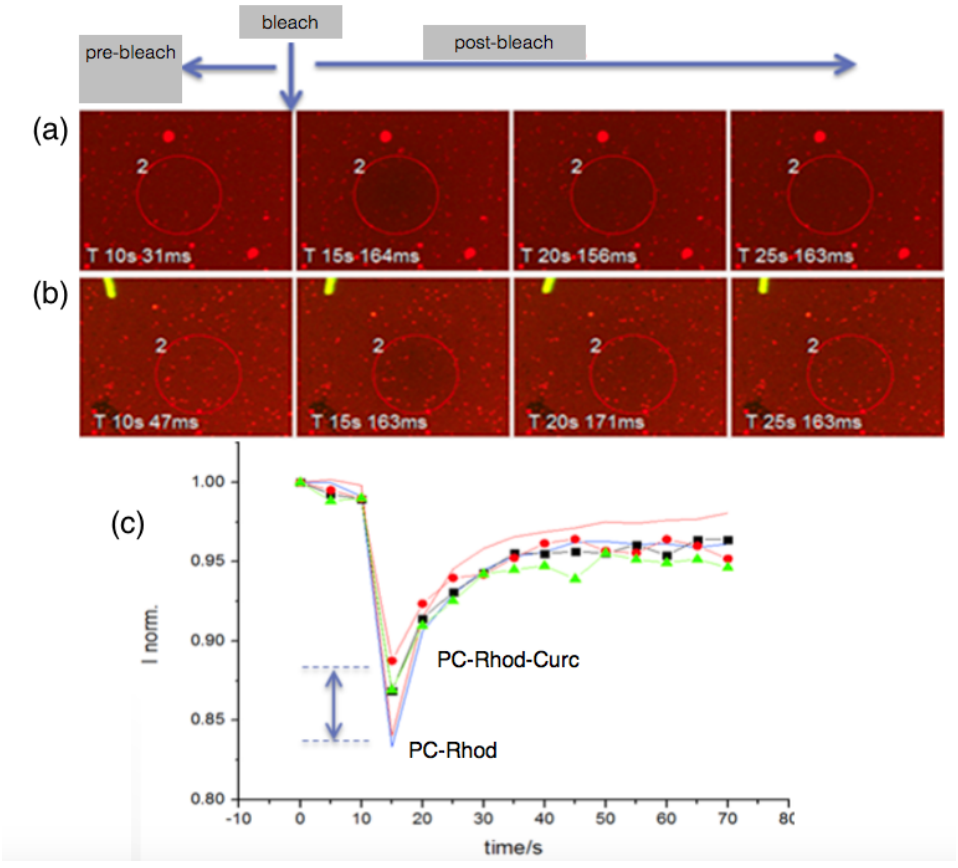

Figure 8. Confocal microscopy and FRAP analysis of rhodamine-labelled POPC without and with the loading of curcumin. Representative micrographs for FRAP experiments on: (a) POPC-Rhod; (b) POPC-Rhod-Curc. In (c): the curves of normalized emission intensity of rhodamine ($\lambda_{ex/em}$ = 543/550–650 nm) before and after photobleaching (POPC-Rhod = line; POPC-Rhod-Curc = line + symbol).

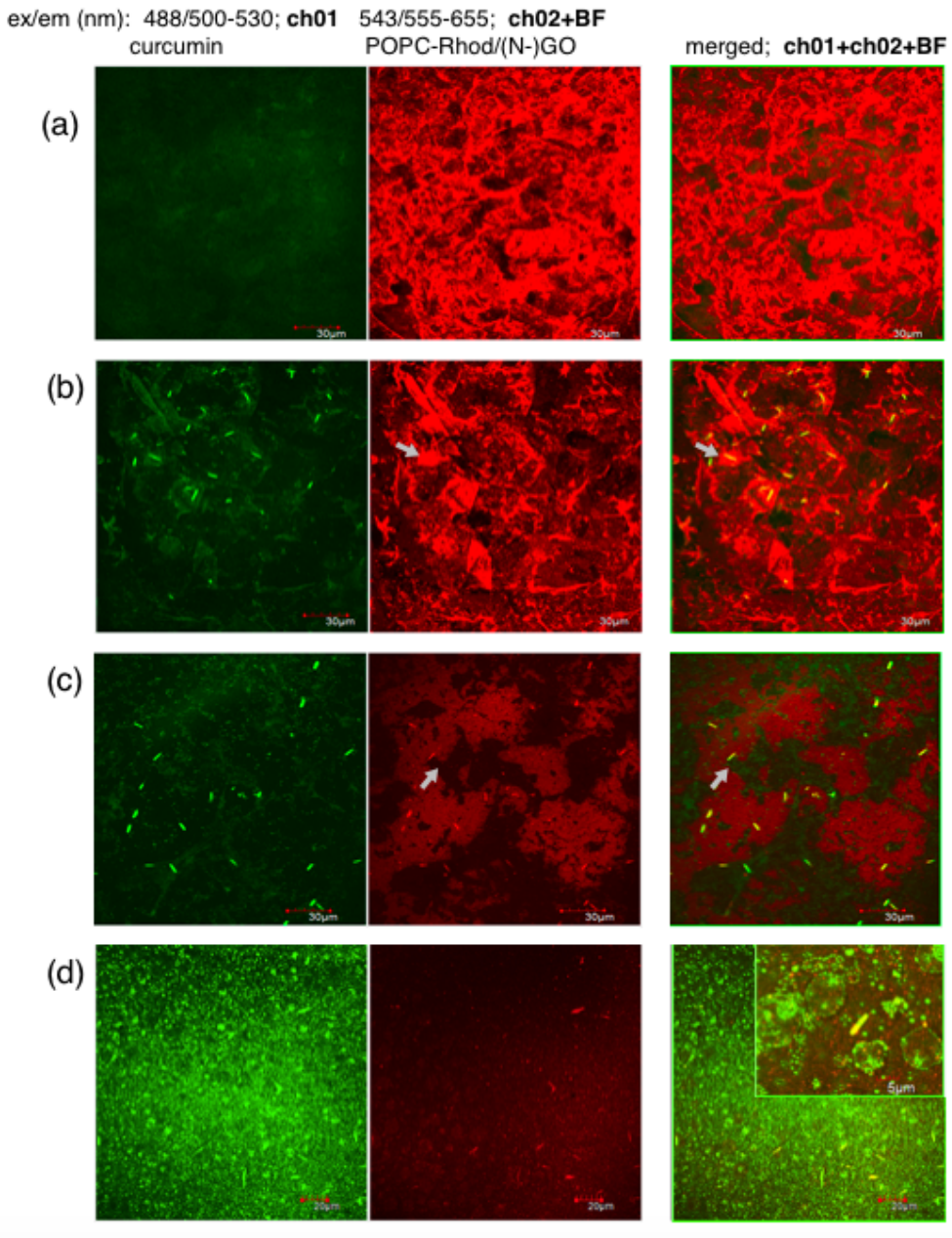

Figure 9. Confocal micrographs and bright field (BF) optical images of POPC-Rhod adsorbed on GO (a) and POPC-Rhod-Curc adsorbed on GO (b), methyl-terminated N-GO (c), amino-terminated N-GO (d). The arrows point to some GO and N-GO sheets.

Figure 8 shows the representative micrographs of the FRAP experiment for PC-Rhod (Figure 8a) and PC-Rhod-Curc (Figure 8b), as well as the curves of normalized intensity before and after the photobleaching (Figure 8c). It must be noted that the minimum, which corresponds to the first scan immediately after the bleach, is less pronounced for the Curc-loaded lipid membrane. This indicates a higher fluidity than the bare SLB. However, the diffusion coefficients, calculated by using the Axelrod's algorithm ($D = 0.88w^2/4\tau_{1/2}$, where w is the radius of the bleached area and $\tau_{1/2}$ describes time for 50% recovery [42]) is about 1.6–1.7 (±0.2) $\mu m^2/s$ for both PC-Rhod and PC-Rhod-Curc.

The confocal microscopy images for POPC-Rhod or POPC-Rhod-Curc adsorbed onto the different GO and N-GO substrates, prepared by the approach with GO solid, are shown in Figure 9.

The inhomogeneous distribution of red emission from the POPC-Rhod lipids highlights the graphene sheets (see the contrast in the merged fluorescence and optical images, ch02 + BF) in the hybrid glass-GO samples. The curcumin fluorescence is clearly visible on the different GO and N-GO sheets, with a particular enhancement of the green fluorescence on the top surface of the N-GO sheets prepared by dodecylamine reduction (Figure 9c, see the merged fluorescence and optical images, ch01 + ch02 + BF). This finding could be explained by the higher affinity of the hydrophobic curcumin towards the methyl-terminated N-GO sheets in comparison to the hydrophilic GO. According to that, the much larger regions with evident darker contrast in the red emission (Figure 9c, image ch02 + BF) fit well with a less favoured process of supported lipid bilayer formation from the spontaneous adsorption-rupture-fusion processes, as expected on a hydrophobic substrate [43]. Interestingly, for the amino-terminated N-GO surfaces the transfer of the drug to the substrate seems even more efficient, as demonstrated by the extensive green fluorescence (Figure 9d, see image ch01). Moreover, an effect similar to the reported formation of curcumin—induced lipid domains [44], with the localization of the drug at the domain boundaries, is also visible (see inset in Figure 9d).

4. Conclusions

In summary, in the present work we investigated two functionalization strategies for graphene oxide in aqueous dispersion and for solid graphene, to prepare N-doped GO with different surface termination (e.g., outward exposure of methyl or NH_2 groups). The experimental characterisation by Raman, UV-visible and XPS spectroscopies demonstrated the actual modification of the GO, and allowed for the N-doping quantification. The interfaces established between such systems and curcumin-loaded lipid membranes was scrutinised by means on theoretical calculations, to elucidate both on the actual surface termination of the various GO samples at the interface with the lipid-curcumin system and on the pH-triggered release process of the curcumin. Experimental results validated the calculations as far as concerns the fluidity of the lipid bilayer (and the consequent freedom degrees of the curcumin intercalated within the membrane) and the promising potentialities for the drug-release at the GO-lipid membrane interface, as demonstrated by the confocal microscopy studies. Further studies will elucidate on the impact of the used strategy for the modulation of the curcumin delivery at the graphene surfaces and the advantages of using the hybrid graphene oxide/lipid bilayer assembly for the release of the hydrophobic drug driven by specific chemical or physical stimuli.

Acknowledgements

Authors acknowledge University of Catania (FIR 2014 grant Cod.018B9A); C.S. and P.D.P. acknowledge PON02_00355_HIPPOCRATES and Consorzio Interuniversitario di Ricerca in Chimica dei Metalli nei Sistemi Biologici (C.I.R.C.M.S.B.).

Conflict of Interest

The authors declare that there is no conflict of interest regarding the publication of this manuscript.

References

1. Rui L, Liu J, Li J, et al. (2015) Reduced graphene oxide directed self-assembly of phospholipid monolayers in liquid and gel phases. *BBA-Biomembranes* 1848: 1203–1211.
2. Ali MA, Kamil RK, Srivastava S, et al. (2014) Lipid-lipid interactions in aminated reduced graphene oxide interface for biosensing application. *Langmuir* 30: 4192–4201.
3. Makharza S, Cirillo G, Bachmatiuk A, et al. (2013) Graphene oxide-based drug delivery vehicles: Functionalization, characterization, and cytotoxicity evaluation. *J Nanopart Res* 15: 2099–2124.
4. Shen H, Zhang L, Liu M, et al. (2012) Biomedical applications of graphene. *Theranostics* 2: 283–294.
5. Sawosz E, Jaworski S, Kutwin M, et al. (2015) Graphene functionalized with arginine decreases the development of glioblastoma multiforme tumor in a gene-dependent manner. *Int J Mol Sci* 16: 25214–25233.
6. Lei H, Zhou X, Wu H, et al. (2014) Morphology change and detachment of lipid bilayers from the mica substrate driven by graphene oxide sheets. *Langmuir* 30: 4678–4683.
7. Yang K, Feng L, Shi X, et al. (2013) Nano-graphene in biomedicine: theranostic applications. *Chem Soc Rev* 42: 530–547.
8. Novoselov KS, Fal'ko VI, Colombo L, et al. (2012) A roadmap for graphene. *Nature* 490: 192–200.
9. Loh KP, Bao Q, Eda G, et al. (2010) Graphene oxide as a chemically tunable platform for optical applications. *Nat Chem* 2: 1015–1024.
10. Seabra AB, Paula AJ, de Lima R, et al. (2014) Nanotoxicity of graphene and graphene oxide. *Chem Res Toxicol* 27: 159–168.
11. Liu X, Chen KL (2015) Interactions of graphene oxide with model cell membranes: Probing nanoparticle attachment and lipid bilayer disruption. *Langmuir* 31: 12076–12086.
12. Yi P, Chen KL (2013) Interaction of multiwalled carbon nanotubes with supported lipid bilayers and vesicles as model biological membranes. *Environ Sci Technol* 47: 5711–5719.
13. Frost R, Jönsson GE, Chakarov D, et al. (2012) Graphene oxide and lipid membranes: Interactions and nanocomposite structures. *Nano Lett* 12: 3356–3362.
14. Wang Z, Dong Y, Li H, et al. (2014) Enhancing lithium-sulphur battery performance by strongly binding the discharge products on amino-functionalized reduced graphene oxide. *Nat Commun* 5: 5002–5009.
15. Fazaeli Y, Akhavan O, Rahighi R, et al. (2014) In vivo SPECT imaging of tumors by $^{198, 199}$Au-labeled graphene oxide nanostructures. *Mater Sci Eng C* 45: 196–204.
16. Yang X, Mei T, Yang J, et al. (2014) Synthesis and characterization of alkylamine-functionalized graphene for polyolefin-based nanocomposites. *Appl Surf Sci* 305: 725–731.
17. Rao KS, Senthilnathan J, Ting JM, et al. (2014) Continuous production of nitrogen-functionalized graphene nanosheets for catalysis applications. *Nanoscale* 6: 12758–12768.

18. Chua CK, Sofer Z, Luxa J, et al. (2015) Selective nitrogen functionalization of graphene by bucherer-type reaction. *Chem-A Eur J* 21: 8090–8095.
19. Chaban VV, Prezhdo OV (2015) Synergistic Amination of Graphene: Molecular Dynamics and Thermodynamics. *J Phys Chem Lett* 6: 4397–4403.
20. Zuccaro L, Krieg J, Desideri A, et al. (2015) Tuning the isoelectric point of graphene by electrochemical functionalization. *Sci Rep* 5: 11794–11806.
21. Wu L, Zeng L, Jiang X (2015) Revealing the Nature of Interaction between Graphene Oxide and Lipid Membrane by Surface-Enhanced Infrared Absorption (SEIRA) Spectroscopy. *J Am Chem Soc* 137: 10052–10055.
22. Alok A, Singh ID, Singh S, et al. (2015) Curcumin—Pharmacological actions and its role in oral submucous fibrosis: A review. *J Clin Diagnostic Res* 9: ZE01–ZE03.
23. Chen Y, Wu Q, Zhang Z, et al. (2012) Preparation of curcumin-loaded liposomes and evaluation of their skin permeation and pharmacodynamics. *Molecules* 17: 5972–5987.
24. Cheng YC, Kaloni TP, Zhu ZY, et al. (2012) Oxidation of graphene in ozone under ultraviolet light. *Appl Phys Lett* 101: 073110–073114.
25. Hummers WS, Offeman RE (1958) Preparation of Graphitic Oxide. *J Am Chem Soc* 80: 1339–1339.
26. Ren PG, Wang H, Huang HD, et al. (2014) Characterization and performance of dodecyl amine functionalized graphene oxide and dodecyl amine functionalized graphene/high-density polyethylene nanocomposites: A comparative study. *J Appl Polym Sci* 131: 39803–39811.
27. Lerf A, He H, Forster M, et al. (1998) Structure of Graphite Oxide Revisited. *J Phys Chem B* 102: 4477–4482.
28. Perdew J, Burke K, Ernzerhof M (1996) Generalized Gradient Approximation Made Simple. *Phys Rev Lett* 77: 3865–3868.
29. McLean AD, Chandler GS (1980) Contracted Gaussian basis sets for molecular calculations. I. Second row atoms, Z = 11–18. *J Chem Phys* 72: 5639–5648.
30. Krishnan R, Binkley JS, Seeger R, et al. (1980) Self-consistent molecular orbital methods. XX. A basis set for correlated wave functions. *J Chem Phys* 72: 650–654.
31. Forte G, Travaglia A, Magrì A, et al. (2014) Adsorption of NGF and BDNF derived peptides on gold surfaces. *Phys Chem Chem Phys* 16: 1536–1544.
32. Dauber-Osguthorpe P, Roberts VA, Osguthorpe DJ, et al. (1988) Structure and energetics of ligand binding to proteins: Escherichia coli dihydrofolate reductase-trimethoprim, a drug-receptor system. *Proteins* 4: 31–47.
33. Lau KF, Alper HE, Thacher TS, et al. (1994) Effects of Switching-Functions on the Behavior of Liquid Water in Molecular-Dynamics Simulations. *J Phys Chem* 98: 8785–8792.
34. D'Urso L, Satriano C, Forte G, et al. (2012) Water structure and charge transfer phenomena at the liquid-graphene interface. *Phys Chem Chem Phys* 14: 14605–14610.
35. Bourlinos AB, Gournis D, Petridis D, et al. (2003) Graphite oxide: Chemical reduction to graphite and surface modification with primary aliphatic amines and amino acids. *Langmuir* 19: 6050–6055.
36. Eda G, Lin YY, Mattevi C, et al. (2010) Blue photoluminescence from chemically derived graphene oxide. *Adv Mater* 22: 505–509.
37. Lai Q, Zhu S, Luo X, et al. (2012) Ultraviolet-visible spectroscopy of graphene oxides. *AIP Adv* 2: 032146–032150.

38. Dementjev AP, de Graaf A, Van de Sanden MCM, et al. (2000) X-ray photoelectron spectroscopy reference data for identification of the C_3N_4 phase in carbon-nitrogen films. *Diam Relat Mater* 9: 1904–1907.
39. Petit C, Seredych M, Bandosz TJ (2009) Revisiting the chemistry of graphite oxides and its effect on ammonia adsorption. *J Mater Chem* 19: 9176–9185.
40. Mungse HP, Singh R, Sugimura H, et al. (2015) Molecular pillar supported graphene oxide framework: conformational heterogeneity and tunable d-spacing. *Phys Chem Chem Phys* 17: 20822–20829.
41. Satriano C, Svedhem S, Kasemo B (2012) Well-defined lipid interfaces for protein adsorption studies. *Phys Chem Chem Phys* 14: 16695–16698.
42. Axelrod D, Koppel DE, Schlessinger J, et al. (1976) Mobility measurement by analysis of fluorescence photobleaching recovery kinetics. *Biophys J* 16: 1055–1069.
43. Satriano C, Marletta G, Kasemo B (2008) Oxygen plasma-induced conversion of polysiloxane into hydrophilic and smooth SiO_x surfaces. *Surf Interface Anal* 40: 649–656.
44. Tsukamoto M, Kuroda K, Ramamoorthy A, et al. (2014) Modulation of raft domains in a lipid bilayer by boundary-active curcumin. *Chem Commun* 50: 3427–3430.

AIMS Press